Journal of Applied Mechanics Vol.10, pp.855-864 (August 2007) JSCE

Hydrodynamic Modeling of Pyroclastic Flows

流体力学的手法による火砕流の流動モデル

Norihito Osawa*, Pujirahajo Alwafi**, Yusuke Fukushima*** and Tokuzo Hosoyamada****
大澤 範一・フジラハジョ アルアフィ・福嶋 祐介・細山田 得三

* Member M. of Eng. Tokyo Kensetsu Consultant Co. Ltd. (1-15-6, Kitaotuka, Toshima-Ku, Tokyo 171-0014)
** Member M. of Eng. Department of Civil and Environmental Engineering, Nagaoka University of Technology (1603-1, Kamitomioka, Nagaoka, Niigata 940-2188)
*** Member Dr. of Eng. Prof. Department of Civil and Environmental Engineering, Nagaoka University of Technology (1603-1, Kamitomioka, Nagaoka, Niigata 940-2188)
**** Member Dr. of Eng. Associate Prof. Department of Civil and Environmental Engineering, Nagaoka University of Technology (1603-1, Kamitomioka, Nagaoka, Niigata 940-2188)

Gas-solid two-phase flows occur in a large number of natural phenomena, of which pyroclastic flow is a typical example. Japan has many active volcanoes and thus many regions are vulnerable to disasters caused by pyroclastic flows. In order to prevent these disasters, the understanding on dynamical processes of pyroclastic flow is important. Hazard maps and disaster prevention facilities against pyroclastic flows should be produced based on such knowledge. In this study, a new simulation model of pyroclastic flow based on hydrodynamic principles was proposed. The present simulation model can use a 3-dimensional topography data mesh and analysis flow path and spread width of pyroclastic flows in addition to predicting the main parameters such as flow velocity. And the proposed model applies to real field in Mt. Fugen.

Key Words: *pyroclastic flow, gas-solid two-phase flows, simulation model, 3-dimensional topography*

1. Introduction

Flows consisting of solid particles mixed in gas, referred to as gas-solid two-phase flows, can be observed in a wide variety of phenomena in nature. One of such phenomena is a pyroclastic flow, which is a fluid of pyroclastic materials (e.g., volcanic ash and lapilli) mixed in air that flows down the slope of a volcano after eruption into the air by volcanic activity. The flow of these materials down the mountainside is highly turbulent due to high downstream velocity, causing a fraction of the material to be continually ejected into the air, where some material remains for some time. Because the particles gradually sink to the bottom of the flow, pyroclastic flows reach further distance from the mouth of the volcano.[1)]

Powder-snow avalanches, which occur in particularly cold locations in the mountains in winter, are other example of natural gas-solid two-phase flows. These occur when large numbers of snow particles are suddenly disturbed, usually by the wind, and begin to move down a slope. The motion of powder-snow avalanches closely resembles that of thermals. Fukushima[2)] proposed a method of numerical analysis for powder-snow avalanches by applying the thermal theory in hydrodynamics. Thermal is defined as a currents accelerated by density difference between flowing fluid and ambient homogeneous fluid. Powder-snow avalanches are similar to thermal flows in that the fluid surrounding the flow is entrained into the flow as it proceeds downstream such that the volume increases with downstream. However, powder-snow avalanches differ from thermals in that the latter is a single-layer phenomenon, while the former is a mixture of solid and gas phases, where solid snow particles are entrained from the bottom of the flow while the mass of snow increases with downstream due to the fall of snow particles. Fukushima[2)] examined the mechanisms of powder-snow avalanches using mass conservation equations and succeeded in reproducing the

entire process of explosive growth of the snow mass with distance downstream.

In comparisons of pyroclastic flows with powder-snow avalanches, the snow particles are replaced by pyroclastic materials, but the gas-solid two-phase flows are otherwise very similar, involving mixing of fine solid particles with air, and descent of flow along sloping surfaces. But, there remains one important difference. There is almost no temperature change along the flow path of a powder-snow avalanche, which happens in the coldest part of winter, whereas a pyroclastic flow undergoes a marked change in temperature with downstream; beginning at a very high temperature and cooling as it continues down the side of the volcano. The viscosity of high-temperature air is much higher than that of air at closer to room temperature, slowing the fall of hot suspended pyroclastic materials. Fukushima and Kagiyama[3] proposed an analytical model for pyroclastic flows based on Fukushima's model for powder-snow avalanches, with an additional fundamental equation to account for temperature change. Using actual data recorded in the path of a pyroclastic flow at Mt. Fugen, the final flow distance, abrupt acceleration at eruption and other parameters were successfully reproduced by this extended model.

However, the Fukushima-Kagiyama pyroclastic flow model[3] is a one-dimensional (1D) model, and it is necessary to add data concerning the flow path. Another limitation is that the stream is assumed to be of unit width, that is, the model does not account for the lateral spread of an actual flow. Therefore, it is difficult to incorporate the influence of other factors, such as the frictional coefficient due to the variation in shape of pyroclastic flows. The shape of the flow path and the lateral spread of the stream are critical parameters in disaster mitigation, for which flow models are important in the creation of hazard maps and designing disaster mitigation facilities.

In the present study, the Fukushima-Kagiyama model[3] is used as the foundation for a new model into which a mesh of three-dimensional (3D) site topography data is incorporated. A two-dimensional (2D) analytical model of pyroclastic flows is proposed for predicting the flow path of a pyroclastic flow from any arbitrary point. This model is intended to predict lateral spreading, with an analytical region expanding to include the entire volume, and accounts for friction due to stream shape change and other factors. And the proposed model applies to real field in Mt. Fugen in Unzen mountains in Nagasaki Prefecture. Mt. Fugen erupted in 1990, causing devastating natural disaster.

2. Method of Numerical Analysis

2.1 Definition of analytical model of flow

For convenience in the following explanations, the model proposed by Fukushima and Kagiyama[3] incorporating flow path cross-section data and assuming unit width will be referred to as the 1D model. In this paper, the analytical region is extended laterally to include the entire actual width of a spreading pyroclastic flow, incorporating 3D topographic data, and the eruption is allowed to occur at any arbitrary point on the mountainside. This is referred to as the 2D model.

2.2 Modeling of pyroclastic flows

Beghin et al.[4] performed an experiment examining a simple sloping thermal and showed that the thermal body took on an approximately semi-ellipsoidal shape as it flowed down the experimental slope. Fukushima and Kagiyama employed this result in their 1D model,[3] defining a semi-elliptical cross-section for the pyroclastic body (see Fig. 1). Here, h is the height of the body, P_i is the total length of contact between the pyroclastic body and the air, P_b is the length of contact between the pyroclastic body and the ground surface, ρ is the mean density of the pyroclastic body, and ρ_a is the density of the ambient air.

2.3 Fundamental equations for 2D analytical model

The 1D model is based on Beghin's theory of thermals.[4] The 2D model also applies that theory, with fundamental equations for the continuity of air, mass conservation for pyroclastic materials, kinetic energy of turbulence, heat balance, motion in both directions, location in both directions, and maximum spread width:

· Continuity equation for air

$$\frac{d}{dt}(\rho_0 V_o) = \rho_a E_a U_{abs} S_i \qquad (1)$$

· Mass conservation equation for pyroclastic flow

$$\frac{d}{dt}(CV_o) = v_s\left(E_s - C_b \cos\theta\right)S_b \qquad (2)$$

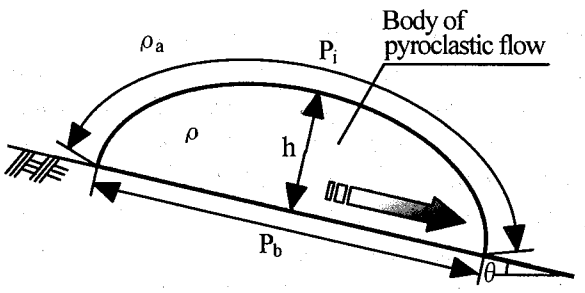

Fig.1 Schematic view of pyroclastic flow

Table 1 Coefficients employed in 2D model of pyroclastic flow

V_o	Volume of pyroc. flow	T	Temperature of pyroc. flow	τ_i	Shear stress at interface with air
h	Height of pyroc. flow	T_a	Ambient temperature	τ_b	Shear stress at interface with ground
P_i	Air contact length	T_b	Temperature near base of flow	α_B	Coef. for max. spread of flow
P_b	Base contact length	E_s	Particle entrainment coef.	R	Spec. gravity, pyroc. materials in air
S_i	Air contact area	E_a	Air entrainment coef.	β	Viscous dissipation rate coef.
S_b	Ground contact area	θ	Slope angle in flow direction	C_D	Coef. of drag
C	Mean conc. of pyroc. materials	θ_x	Slope angle in x direction	ξ	Shape factor
C_b	Base conc. of pyroc. materials	θ_y	Slope angle in y direction	D_s	Dia. of pyroc. materials
U_{abs}	Abs. velocity of flow on path	k_v	Supplementary gravity coef.	r_0	Concentration ratio at base
U_x	x component of velocity	ρ	Density of mixed flow	X	Horizontal x displacement
U_y	y comp of velocity	ρ_a	Air density	Y	Horizontal y displacement
K	Kinetic energy of turbulence	ρ_s	Density of pyroc. materials	S	Displacement of flow
b_{max}	Max. width of flow	v_s	Pyroc. materials fall velocity	γ	Angle from slope to vertical

· Heat balance equation

$$\frac{d}{dt}\{(\rho_0 c_{pa} + \rho_s c_{ps} C)V_o T\} = \rho_a c_{pa} T_a E_a U_{abs} S_i + \rho_s c_{ps} v_s (E_s T_b - C_b \cos\theta T) S_b + \rho\beta \frac{K^{3/2}}{h} V_o \quad (3)$$

· Equation of kinetic energy of turbulence

$$\frac{d}{dt}\{(\rho + k_v \rho_a)KV_o\} = (\tau_i S_i + \tau_b S_b)U_{abs} + \frac{1}{2}\rho_a\{(1+k_v)E_a U_{abs} S_i + R v_s (E_s - C_b \cos\theta) S_b\} U_{abs}^2 - \rho_a R g v_s V_o - \beta\rho K^{3/2} V_o / h - \xi_p \rho_a R g \cos\theta h \times \left\{\frac{1}{2} C E_a U_{abs} S_i + v_s (E_s - C_b \cos\theta) S_b\right\} \quad (4)$$

· Equation of motion, x direction

$$\frac{d}{dt}\{(\rho + k_v \rho_a) U_x V_o\} = (\rho - \rho_a) g V_o \sin\theta_x - (\tau_i S_i + \tau_b S_b)\frac{U_x}{U_{abs}} \quad (5)$$

· Equation of motion, y direction

$$\frac{d}{dt}\{(\rho + k_v \rho_a) U_y V_o\} = (\rho - \rho_a) g V_o \sin\theta_y - (\tau_i S_i + \tau_b S_b)\frac{U_y}{U_{abs}} \quad (6)$$

· Horizontal position equation, x direction

$$\frac{dX}{dt} = U_x \cos\theta_x \quad (7)$$

· Horizontal position equation, y direction

$$\frac{dY}{dt} = U_y \cos\theta_y \quad (8)$$

· Maximum spread width equation

$$\frac{db_{max}}{dt} = \alpha_B (\tan\theta)^{-0.264} U_{abs} \quad (9)$$

In this study, the fourth-order Runge–Kutta method was used to calculate. (Time step was 0.2s.)

The fundamental equations for the previous 1D model and the present 2D model differ in the following ways. Expanding the analytical region to the entire volume of the pyroclastic flow requires some new parameters, including the interface area (S_i), which replaces the interface length (P_i), the area of the base contact surface (S_b), which replaces the length of the contact (P_b), and the pyroclastic flow volume (V_o), which replaces the area at unit flow length (A). For the lateral spread of the flow (Eq. (9)), Fukushima's 3D formula for inclined thermals is employed.[5] As the 2D model handles this parameter as an unknown variables of the downstream flow path, the equations of motion are broken up into vectors in the x and y directions, and fundamental equations are added to represent the horizontal location in both directions.

As mentioned earlier, simple thermal flow is a single-layer phenomenon, while pyroclastic flow is a gas-solid two-phase flow consisting of pyroclastic particles that are constantly entrained from bottom and allowed to free-fall. The total number of particles thus varies constantly along the flow path. This process is evaluated using the mass conservation equation of the flow. The left side of Eq. (2) expresses the time-based changes in the amount of pyroclastic material, and on the right side, the

$v_s E_s S_b$ term expresses the sweeping up of materials from the bottom of the flow and the $v_s C_b \cos\theta S_b$ term expresses the fall of particles back toward the bottom. In a powder-snow avalanche, the slip face for the avalanche is the upper face of the accumulated snow, and it is thus reasonable to imagine that there is continual "entraining particles" of material from that layer with progress along the avalanche path. In pyroclastic flows, however, the slip face is the ground itself. While the conditions of tephra deposition and other factors are likely controlling factors, if the pyroclastic flow is assumed to be an initial flow, entrain of the underlying materials is supposed to be limited. Therefore, it is assumed in this 2D model that there is no increase in the total amount of pyroclastic materials in the flow. Then, Eq. (2) is modified as follows:

$$E_s \geq C_b \cos\theta$$

$$\frac{d}{dt} CV_o = 0 \tag{2.a}$$

$$E_s < C_b \cos\theta$$

$$\frac{d}{dt} CV_o = v_s \left(E_s - C_b \cos\theta\right) S_b \tag{2.b}$$

The 2D model used in this study employs a large number of coefficients, the most important of which are listed in Table 1.

2.4 Constitutive equations for 2D model

As the fundamental equations of the 2D model include many unknowns, the above equations alone are not sufficient to provide solutions. Some additional assumptions are thus made according to the constitutive equations.

Absolute velocity (U_{abs}) can be expressed as

$$U_{abs} = \sqrt{\left\{(U_x + U_y \cos\gamma)^2 + (U_y \sin\gamma)^2\right\}} \tag{10}$$

Here, γ is the angle made by the slope with the vertical axis, and can be expressed by

$$\gamma = \tan^{-1}\left(\frac{U_x \cos\theta_x}{U_y \cos\theta_y}\right) \tag{11}$$

The length of the contact interface between the flow and the ground (P_b) and the length of the interface with the air (P_i) are approximated using the experimental results of Fukushima[2] and Beghin et al.:[4]

$$P_b = \xi_b h \tag{12}$$

$$P_i = \xi_i h \tag{13}$$

$$\xi_i = \frac{\pi}{2\sqrt{2}} \sqrt{(\xi_b^{-2} + 1)} \xi_b \tag{14}$$

$$\xi_b = 8.47\theta^{-1/3} \tag{15}$$

$$\xi_P = 3/4\,\pi \tag{16}$$

$$k_v = 2/\xi_b \tag{17}$$

The shape of the flow is also assumed to be semi-ellipsoidal in the lateral direction. The flow volume (V_o) and the area of contact with the ground (S_b) and air (S_i) are then given by the following geometric relations:

$$V_o = \left(\frac{\pi}{6}\right) P_b b_{max} h \tag{18}$$

$$S_b = (\pi/4) P_b b_{max} \tag{19}$$

$$S_i = \alpha_1 S_b \tag{20}$$

where α_1 is a correction factor with value of 1 or higher.

The shear stresses at the ground surface (τ_b) and at the interface with the air (τ_i) are given by

$$\tau_b = \rho_b \alpha K \tag{21}$$

$$\tau_i = \rho_a \alpha K \tag{22}$$

where α is the dimensionless coefficient of friction.

The dimensionless coefficient for viscous dissipation rate (β), the friction coefficient (α), and the drag coefficient (C_D) associated with the molecular viscosity dissipation ratio are related by the following expression:

$$\beta = \frac{1}{\xi_A}\left(\frac{\alpha}{C_D}\right)^{3/2} \left\{(\xi_i + \xi_b) C_D + \left(1 - \frac{C_D}{\alpha}\right)\frac{1}{2}(1 + k_v)\xi_i E_a + \xi_P \cot\theta \frac{\xi_i E_a}{2\xi_A}\left[\frac{3}{4}(1 + k_v)\xi_i E_a + (\xi_i + \xi_b) C_D\right]\right\} \tag{23}$$

C_D can be approximated by Schiller's equation (see Graf[6]):

$$C_D = \frac{24}{\mathrm{Re}}\left(1 + 0.150\,\mathrm{Re}^{0.687}\right) \tag{24}$$

where the Reynolds number (Re) is given by the following expression using the kinematic viscosity of the air (υ) and particle diameter (D_s):

$$\mathrm{Re} = \frac{D_s v_s}{\upsilon} \tag{25}$$

Table 2 Influence of pyroclastic particle diameter and temperature on fall velocity and other properties

D_s (mm)	T (℃)	υ (cm²/s)	ρ_0 (g/cm³)	v_s (cm/s)	Re
0.10	1,000	1.73	2.76×10^{-4}	28.8	0.17
0.15				61.7	0.53
0.20				102.0	1.19
0.30				200.2	3.46
0.40				305.8	7.06
0.50				412.7	11.90
0.10	20	0.15	1.20×10^{-3}	58.1	3.89
	250	0.41	6.74×10^{-4}	45.4	1.12
	500	0.78	4.56×10^{-4}	37.3	0.48
	750	1.22	3.45×10^{-4}	32.5	0.27
	1,000	1.73	2.76×10^{-4}	28.8	0.17

The fall velocity of the pyroclastic materials is estimated by assuming equilibrium between the particle weight and the drag of the particle in the air. The equilibrium equation is as follows:

$$C_D\pi\frac{D_s^2}{8}\rho_a v_s^2 = \pi\frac{D_s^3}{6}(\rho_s-\rho_a)g \qquad (26)$$

It is clear from relations (24)–(26) that v_s varies with particle diameter (D_s) and temperature (T). Table 2 shows how the air density (ρ_0), air kinematic viscosity (υ), fall velocity (v_s), and the Reynolds number of particles vary with T and D_s. The air density can be estimated by the following equation with temperature in degrees Celsius:

$$\rho_0 = \frac{0.001293}{1+0.00367\ T} \qquad (27)$$

In the air with density (ρ_0), the specific gravity (R) of pyroclastic materials is expressed as

$$R = (\rho_s - \rho_0)/\rho_0 \qquad (28)$$

The mean density of the pyroclastic flow (ρ) and the density of the base (ρ_b) are found using the following relations and the parameters of specific gravity of the pyroclastic materials (R), the mean concentration of the pyroclastic materials (C), and the mean concentration of the materials at the base (C_b).

$$\rho = \rho_0(1+RC) \qquad (29)$$

$$\rho_b = \rho_0(1+RC_b) \qquad (30)$$

Here the ratio between the base density and the mean density (r_0) is calculated with Parker's equation[7] which is originally proposed for open water channels flow with suspended sediments.

$$r_0 = C_b/C = 1+31.5\mu^{-1.46} \qquad (31)$$

$$\mu = \sqrt{\alpha K}/v_s \qquad (32)$$

The surrounding air is entrained into the pyroclastic flow as the flow proceeds. Although the flow grows wider, if the slope is steep, the air entrainment coefficient (E_a) is approximated using the experimental results of turbulent thermals of Escudier et al.:[8]

$$E_a = 0.1(\theta/90°) \qquad (33)$$

Fukushima and Kikuchi et al.[9] showed that as long as the diameter of snow particles is set to an appropriate value, the entrainment coefficient of snow particles into wind-blown snow streams is well represented by the equation obtained by Garcia[10] for open water channels flow with suspended sediments. As pyroclastic flows and wind-blown snow are both gas-solid two-phase flows involving fine particles in air, it is assumed for this study that Garcia's equation[10] can be applied to find the coefficient of entrainment of pyroclastic materials (E_s):

$$E_s = \frac{A_1 Z^5}{\left(1+\frac{A_1}{0.3}Z^5\right)} \qquad (34)$$

where Z is a dimensionless coefficient defined by

$$Z = R_P^{0.6}u_*/v_s \qquad (35)$$

R_P is the Reynolds number of the particles for a given particle diameter, and u_* is the frictional velocity:

$$R_P = \sqrt{RgD_s}D_s/\upsilon \qquad (36)$$

$$u_* = \sqrt{(\tau_b/\rho_b)} \qquad (37)$$

2.5 Modeling the shape of the slope

As pyroclastic flows generally occur near the mouth of a volcano, the slope downstream is usually very steep, and the topography is complicated. The proposed 2D model employs topographic mesh data as the altitude condition of the studied area. When this is used to represent a given slope from a space, the simplest method is to divide the topographic mesh into finer triangular elements (Fig. 2). Fukushima and Hayakawa have proposed a method for deriving the slope parameters of the small triangular elements obtained after subdivision of a topographic mesh.[11] The local gradients (θ_x ,θ_y) of an element are given by the following equations (see Fig. 3):

$$\theta_x = \tan^{-1}\left[(\sin\theta_0 \cos\phi)/\cos\theta_0\right] \quad (38)$$

$$\theta_y = \tan^{-1}\left[(\sin\theta_0 \sin\phi)/\cos\theta_0\right] \quad (39)$$

Here, ϕ is the angle from the x axis to the ray representing the location of the steepest gradient on the element (S in Fig. 3), and θ_0 is the angle of that gradient. Due to inertia and other factors, the flow may not necessarily follow the steepest gradient (s in Fig.3). ϕ is the angle made by the direction of flow to the x axis. The angle of the actual flow with respect to the vertical (θ) can be found by the following geometrical relation:

$$\theta = \tan^{-1}\{\cos(\phi - \psi)\tan\theta_0\} \quad (40)$$

The properties of the slope were derived in this study for the 2D model of pyroclastic flow as follows. It is assumed that the motion of the pyroclastic flow experiences some averaging effect of the complex and varying slope of the surface. It is also assumed that the slope characteristics of the ground underlying the pyroclastic body and ahead of its center have a greater effect on the flow than the ground above (upstream of) the center of the body. Therefore, the portion of the topographic mesh that is downstream of the center, assuming a semi-ellipsoidal shape for the flow body, is re-evaluated and sub-divided into triangular elements (Fig.4). The resulting fine elements are evaluated using Eqs. (38)–(40) to find θ_{xi} ,θ_{yi} and θi . The mean gradient of all these elements under the forward portion of the pyroclastic body is then found using the following expressions (assuming a total of n elements):

$$\theta_x = \frac{1}{n}\sum_{i=1}^{n}\theta_{xi} \quad (41)$$

$$\theta_y = \frac{1}{n}\sum_{i=1}^{n}\theta_{yi} \quad (42)$$

$$\theta = \frac{1}{n}\sum_{i=1}^{n}\theta_i \quad (43)$$

Although the local gradients of the element identified by Eqs. (38)–(40) are discontinuous with those of neighboring elements, such errors can be reduced by using smaller elements.

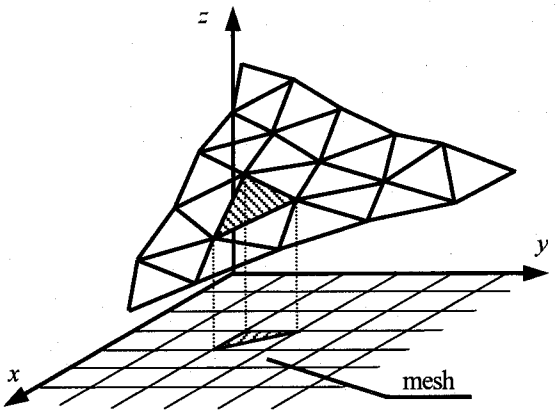

Fig.2 Expression of slope using triangular elements

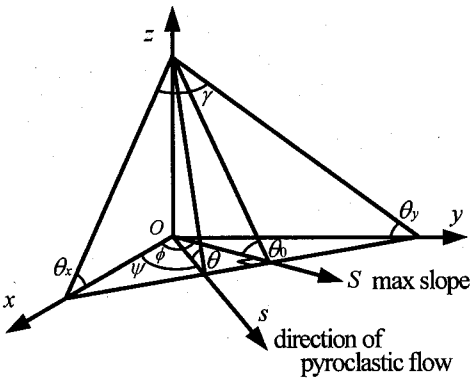

Fig.3 Digitization of sloping shape

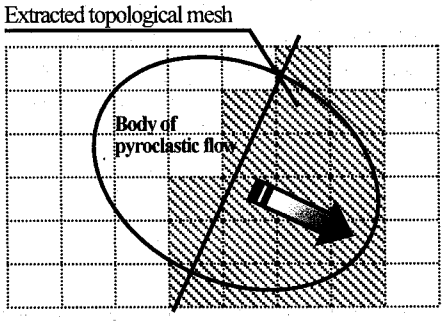

Fig.4 Extraction of topological mesh at tip of pyroclastic flow

3. Results of numerical analysis

3.1 Analytical conditions

(1) Topological data

This model was applied using a numerical simulation of actual topographic data, the 50 m digital national land information mesh for the vicinity of the Mt. Fugen volcano in Nagasaki Prefecture, which erupted in 1990 releasing several pyroclastic flows. Of particular note was the disastrous flow of June, 1991, which took 43 lives, including those of journalists.[12] Activity at Mt. Fugen continued through 1995, resulting in the formation of a new peak, Mt. Heisei Shinzan, and other major topographical changes. The topographic mesh used for the analysis in this study is true to the landforms after those changes. The pyroclastic flows were assumed to originate near the peak of Mt. Heisei Shinzan.

(2) Initial conditions for pyroclastic flow

Table 3 shows the initial conditions assumed for the pyroclastic flows. It is assumed that the pyroclastic materials are blown straight upward and then flow down the slope of the mountain. Therefore the initial flow velocity are $U_{abs\,0} = U_{x0} = U_{y0} = 0$ m/s. The predicted lateral spread (Eq. (9)) is strongly influenced by parameter α_B, which is set to 0.05 considering actual deposition of pyroclastic materials.[12] As the most accurate value for the pyroclastic particle diameter is unknown, 4 values are tested: D_s = 0.1, 0.2, 0.3, and 0.4 mm, and the influence of this parameter is discussed by comparison of the results later.

Table 3 Initial conditions for pyroclastic flow

Initial maximum flow height h_0	50 m
Initial maximum width $b_{max\,0}$	100 m
Initial pyroc. material concentration C_0	5%
Initial temperature T_0	1,000 ℃
Initial flow velocity U_{abs0}	0 m/s

3.2 Results of numerical analysis

The flow distance, maximum height, and maximum flow velocity are given in Table 4. Fig.5 shows a 3D view of the paths predicted for three of the flows down Mt. Fugen using the available topographic data. Fig.6 shows the variations in the horizontal width of the flow assuming an ellipsoidal shape. Fig.7-12 shows the variation of main parameter against the horizontal distance.

(1) Results of numerical analysis under principal conditions

Table 4 and Fig. 7–12 present the following findings.

a) Fig.7 indicates that, in all cases, the pyroclastic flow proceeds from very steep locations to locations with much gentler slopes.

b) Fig.9 predicts that the flow paths vary greatly with particle diameter (D_s). When the particles are large, the fall speed of particles within the flow is faster, and there is a rapid decrease in the total mass of the flow, resulting in a corresponding decrease in the gravity term in the equation of motion, $(\rho - \rho_a)gV_o \sin\theta_x$, and kinetic energy, increasing the relative weight of the shear stresses. Due to these processes, in Case 4, almost no downhill flow was predicted, while in Case 1, the flow accelerated to a maximum of ca. 90 m/s (see Table 4).

c) Comparison of Fig.9 and 11 shows shape of temporal distribution of flow velocity and kinetic energy of turbulence (K) are accordant.

d) Fig.8 indicates a much greater height for Case 1 than for the other cases, attributable to the higher peak flow velocity and lower deceleration with progress along the flow path. Thus, much more of the ambient air was entrained in the flow (Eq. (1) governs the phenomena), resulting in a large total volume. The flow exhibited almost no acceleration in Case 4, and the height never exceeded the initial height of 50 m.

e) Fig.10 shows that the larger the particle diameter (D_s), the more abrupt the fall in temperature with progress along the flow path. The drop of temperature in the present model is mainly due to the falling of hot particles to the ground. Because of this, when particles are large, the fall of particles occurs faster, and the temperature drops more quickly.

Table 4 Results of numerical simulation

	D_s (mm)	S (m)	h (m)	U_{abs} (m/s)
Case1	0.10	6,497	172.1	89.5
Case2	0.20	4,156	66.5	52.6
Case3	0.30	5,833	63.1	27.6
Case4	0.40	293	-*	8.1

*) Height never exceeded the initial value of 50 m in Case 4

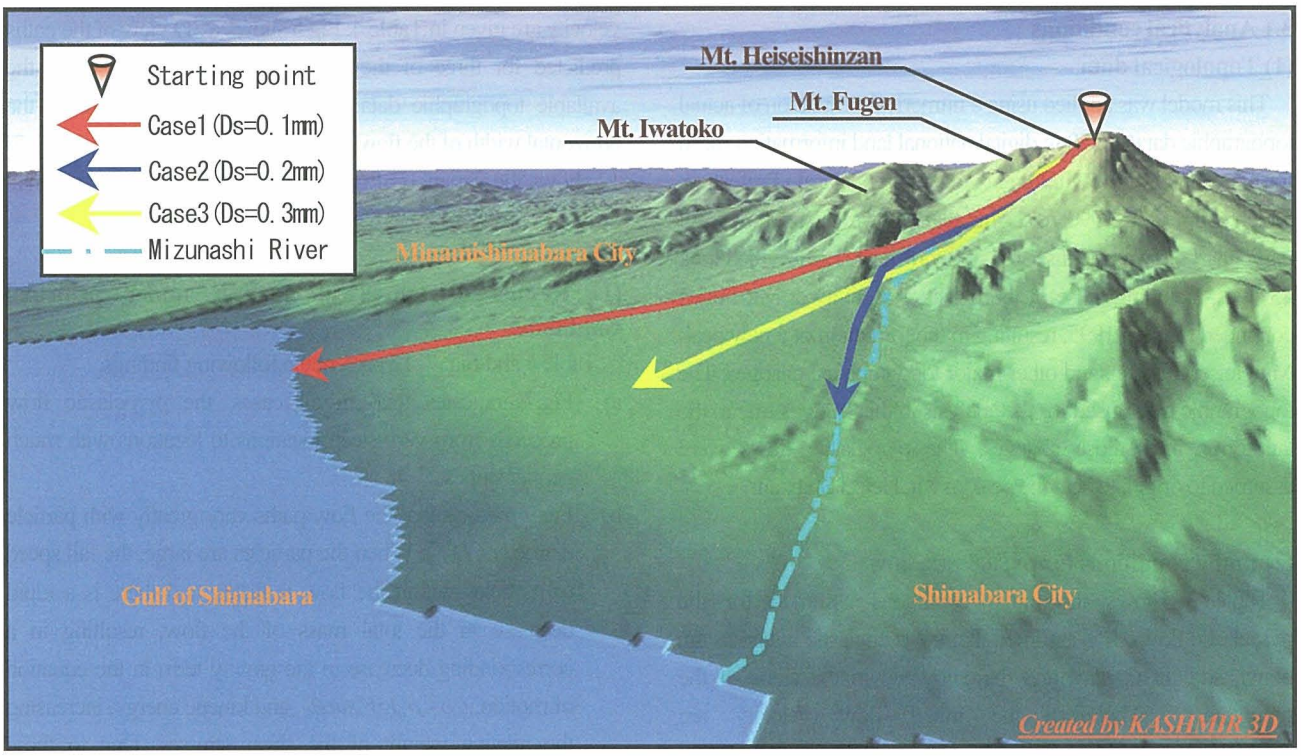

Fig.5 Centerlines of pyroclastic flows predicted by numerical simulation

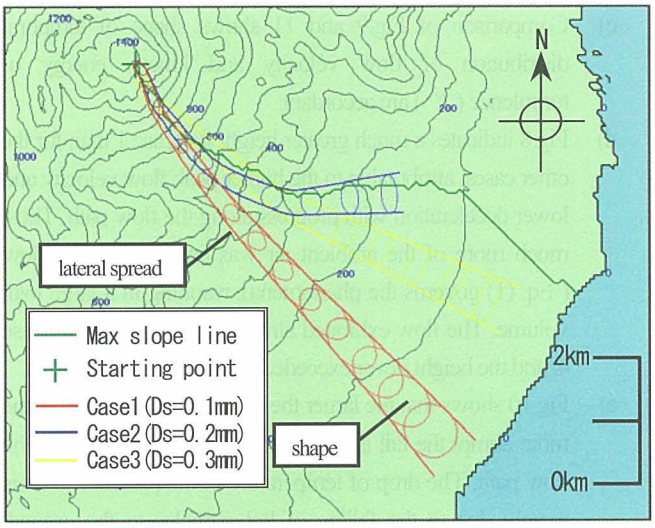

Fig.6 Changes in width and shape of pyroclastic flow

f) Fig.12 reveals an exponential reduction in the concentration of pyroclastic materials in the flow in all cases. Although no increase in the total amount of pyroclastic materials in the flow was allowed in the mass conservation equation, the flow volume grew with progress down its path due to entrainment of ambient air.

(2) Flow path of pyroclastic flow

Fig.6 shows considerable widening of the body of pyroclastic materials, which is assumed to be semi-ellipsoidal, and particularly prominent widening in Case 1, for which the particles were the smallest among the cases. This is because the velocity was higher in the other cases, and the volume increase was greater. The flow width estimated using Eq. (9) predicts a monotonic increase, which is typical for observed pyroclastic flows.

Fig.5 and 6 also indicate that the ultimate flow paths differed considerably due to particle diameter (D_s). With D_s = 0.1 mm, the flow was predicted to continue straight to its endpoint with almost no changes in direction (i.e., to the southeast). In contrast, with D_s = 0.2 mm, the flow proceeded approximately 2000 m down the mountainside, but then made a sharp turn from southeast to east, following the steepest local slope on the mountain. As Fig. 9 clearly shows, the speed in Case 1 was so high that it actually ran upslope at Mt. Iwatoko (see Fig. 5), then began dropping again, still in the southeast direction. In Case 2, however, the speed was lower than in Case 1, and was thus unable to overcome any slopes, turning to follow the steepest slope. The route for Case 3 also differed from the other routes. As larger particles fall back into the flow much faster than small ones, the speed of the flow is reduced. Therefore, the initial speed of Case 3 was lower than in the preceding cases, and the

flow was thus strongly influenced by the greatest gradient of the slope (see Fig. 6). Therefore, there were no topographical features such as Mt. Iwatoko to present any important obstacles to the flow, and the flow never turned as predicted in Case 2. Instead, the flow continued southeast. As Fig. 9 shows, the flow in Case 2 decelerated after approximately 2000 m of horizontal travel, while in Case 3, there was no great deceleration and the flow was faster than in Case 2. The total length in Case 3 was over 1500 m greater than in Case 2.

The existing 1D model employs topographic data from the downstream path and is thus unable to predict the influence of complicated topographic features on the flow. However, the extension of that model to the present 2D version allows such features to be taken into account, providing more realistic reproduction of pyroclastic flows.

(3) Comparison of numerical results with field phenomena

In 1991 the actual pyroclastic flow ran down along Mizunashi River (see Fig. 5).[12] In the numerical results of Case2, the flow path was similar to actual pyroclastic flow in 1991. By using patterns of the destruction, the maximum velocity of the actual flow is estimated to be 50–70 m/s, which is consistent with that predicted by the numerical results for Case 2 (52.6 m/s). Also, difference of stopping position between numerical result for Case2 and field result is small enough.

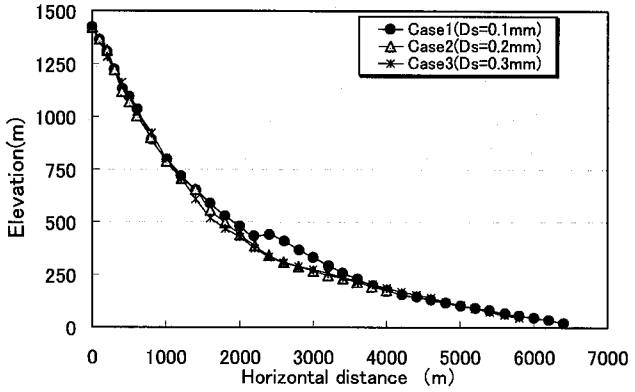

Fig.7 Variation of elevation against the horizontal distance

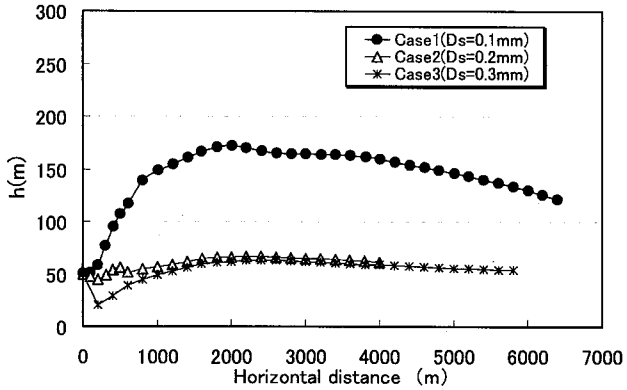

Fig.8 Variation of height against the horizontal distance

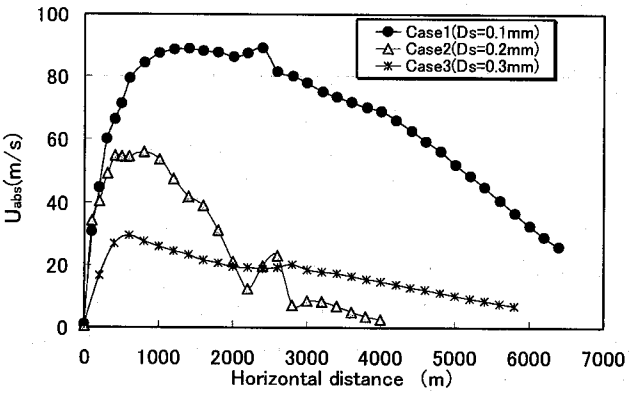

Fig.9 Variation of absolute velocity against the horizontal distance

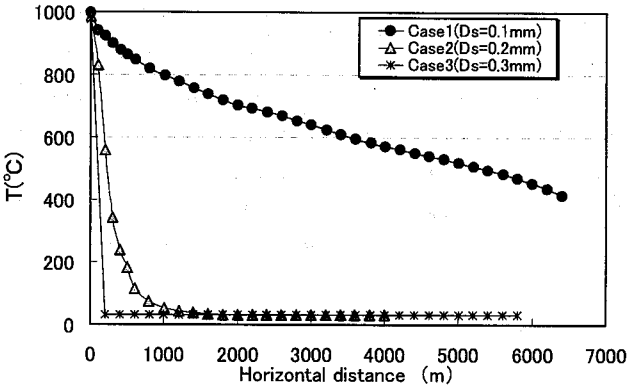

Fig.10 Variation of temperature in the pyroclastic flow against the horizontal distance

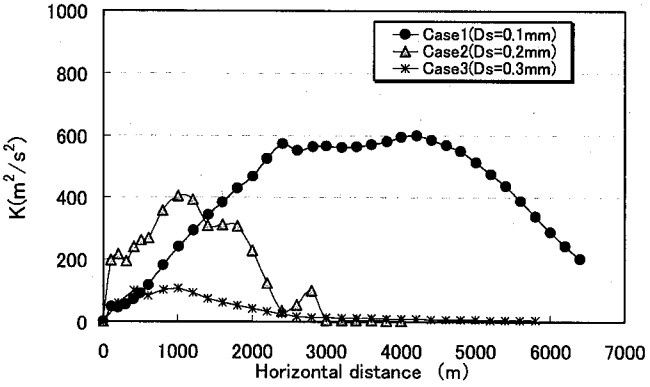

Fig.11 Variation of kinetic energy of turbulence against the horizontal distance

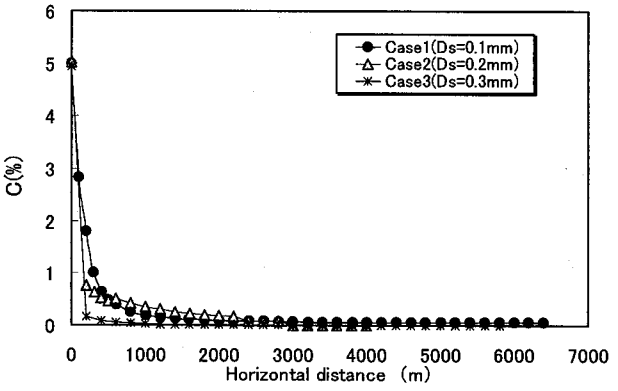

Fig.12 Variation of concentration of pyroclastic materials against the horizontal distance

4. Conclusions

A 2D model of pyroclastic flows was constructed and employed to investigate the flow prediction for different pyroclastic particle sizes using actual topographical data from the Mt. Fugen volcano. This simulation indicated that particle size has a great influence not only on the most important parameters of speed and height of the flow, but also on the path taken by the flow. With appropriate selection of the particle size, the path of the pyroclastic flow from the Mt. Fugen eruption and abrupt acceleration observed immediately following the eruption were successfully simulated numerically. The 2D pyroclastic flow model proposed in this study is applicable to prediction of flow paths and changes the shape, and representing essential information for the creation of hazard maps. At present, the model relies on many assumptions concerning the constitutive equations, dimensionless coefficients, and other conditions. If more field data can be gathered and examined, and further experiments conducted, the constitutive equations and coefficients can be refined, thereby improving the accuracy of this model.

REFERENCES

1) Takahashi, T., Developmental and flow mechanism of pyroclastic flow, Annuals of Disas. Prev. Res. Inst., Kyoto Univ., No.28, pp.1-14, 1985.
2) Fukushima, Y., Analytical study of powder snow avalanches, Seppyo (Journal of the Japanese Society of Snow and Ice), Vol. 48, No. 4, pp. 189-197, 1986.
3) Fukushima, Y., Kagiyama, T., Fluid dynamical simulation model of pyroclastic flow and its application to Mt. Fugen, Unzen Volcano, Kazan, Vol. 37, No. 4, pp. 159-166, 1992.
4) Beghin, P., Hopfinger, E. J., Britter, R. E. : Gravitational convection from instantaneous sources on inclined boundaries, J. Fluid Mech. , No.107, pp.407-422, 1981.
5) Fukushima, Y., Hayakawa, N., Bizen, T., Dynamics of three-dimensional inclined thermal, Proc. of Japan Society of Civil Engineers, No. 473/II-24, pp. 17-24, 1993.
6) Graf, W. H., Hydraulics of Sediment Transport, Water Resources Publications, pp.40-42, 1984.
7) Parker, G., Condition for the ignition of catastrophically erosive turbidity currents, Marine Geology, No.46, pp.307-327, 1982.
8) Escudier, M. P., Maxworthy, T., On the motion of turbulent thermals, J. Fluid Mech., Vol.61, No.3, pp. 541-552, 1973.
9) Fukushima, Y., Kikuchhi, T., Nishimura, K., Snow Entrainment Coefficient of Snowdrifts, Seppyo (Jour. of the Japanese Society of Snow and Ice, Vol. 64, No. 5, pp. 533-540, 2002.
10) Garcia, M., Depositing and eroding sediment driven flows : turbidity currents, St. Anthony Falls Hydraulic Lab., Univ. of Minnesota, Project Report, No.306, pp.179, 1990.
11) Fukushima, Y., Hayakawa, N., Analysis of powder snow avalanches using three-dimensional topographical data, Seppyo (Journal of the Japanese Society of Snow and Ice), Vol. 54, No. 1, pp. 19-26, 1992.
12) Simoturu, D., Hakuno, M., Natural disaster and prevention of disaster, Japan Society for the Promotion of Science, pp.23-53, 1995.

(Received: April 12, 2007)